

Graphical Abstract

To create your abstract, type over the instructions in the template box below.

Fonts or abstract dimensions should not be changed or altered.

Synthesis, crystal structure and complexation behaviour study of an efficient Cu^{2+} ratiometric fluorescent chemosensor based on thiacalix[4]arene

Leave this area blank for abstract info.

Jiang-Lin Zhao,^a Hirotsugu Tomiyasu,^a Chong Wu,^a Hang Cong,^{a,b} Xi Zeng,^b Shofiur Rahman,^c Paris E. Georghiou,^c David L. Hughes,^d Carl Redshaw^c and Takehiko Yamato^{*a}

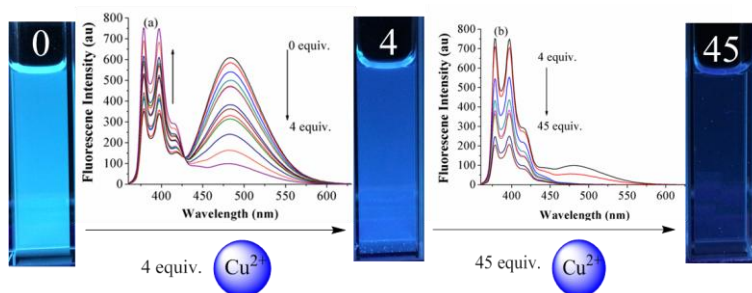
^a *Department of Applied Chemistry, Faculty of Science and Engineering, Saga University, Honjo-machi 1, Saga 840-8502, Japan*

^b *Key Laboratory of Macrocyclic and Supramolecular Chemistry of Guizhou Province, Guizhou University, Guiyang 550025, People's Republic of China*

^c *Department of Chemistry, Memorial University of Newfoundland, St. John's, Newfoundland and Labrador, Canada A1B3X7.*

^d *School of Chemistry, University of East Anglia, Norwich, NR4 7TJ, UK.*

^e *Department of Chemistry, The University of Hull, Cottingham Road, Hull, Yorkshire, HU6 7RX, UK*



Synthesis, crystal structure and complexation behaviour study of an efficient Cu²⁺ ratiometric fluorescent chemosensor based on thiacalix[4]arene

Jiang-Lin Zhao^a, Hirotsugu Tomiyasu^a, Chong Wu^a, Hang Cong^{a,b}, Xi Zeng^b, Shofiu Rahman^c, Paris E. Georghiou^c, David L. Hughes^d, Carl Redshaw^e, Takehiko Yamato^{a,*}

^a Department of Applied Chemistry, Faculty of Science and Engineering, Saga University, Honjo-machi 1, Saga 840-8502, Japan

^b Key Laboratory of Macrocyclic and Supramolecular Chemistry of Guizhou Province, Guizhou University, Guiyang 550025, People's Republic of China

^c Department of Chemistry, Memorial University of Newfoundland, St. John's, Newfoundland and Labrador, Canada A1B3X7.

^d School of Chemistry, University of East Anglia, Norwich, NR4 7TJ, UK.

^e Department of Chemistry, The University of Hull, Cottingham Road, Hull, Yorkshire, HU6 7RX, UK

ABSTRACT

A new thiacalix[4]arene based fluorescent chemosensor **L** bearing two pyrenyl groups in a 1,3-*alternate* conformation has been synthesized, and its metal ion-binding and fluorescence-sensing properties were investigated in ethanol. The designed chemosensor **L** exhibited high selectivity toward Cu²⁺ ions *versus* other tested metal ions with a detection limit of up to 1.44×10^{-7} M. The chemosensor **L** was capable of acting as an efficient ratiometric fluorescent chemosensor at low ion concentration or as a fluorescence quenching type chemosensor due to the PET and heavy atom effects operating in high ionic strength solution. Further studies revealed that chemosensor **L** acted as a reversible sensor in the presence of Cu²⁺ and ethylenediamine.

1. Introduction

Copper is the third most abundant essential trace element in the human body and plays a critical role in various biological processes.¹ For example, copper is a catalytic cofactor for a variety of metalloenzymes, including superoxide dismutase, cytochrome oxidase and tyrosinase.^{1,2} However, it can often be toxic to certain biological systems when the levels of Cu²⁺ exceed cellular needs. Excess levels of the copper (II) ion in the human body can cause kidney damage, gastrointestinal problems and Wilson's disease,³ and are associated with brain diseases such as Parkinson's, Huntington's, Alzheimer's and prion diseases, even when present in trace amounts.^{1c,4} Consequently, the U.S. Environmental Protection Agency (USEPA) has set the limit of copper in drinking water to be 1.3 ppm (~20 μM). Also, the average concentration of blood copper in the normal group is 100–150 μg/dL (15.7–23.6 μM).⁵

In view of the importance of the copper ion, Cu²⁺ selective sensors have been developed recently.^{6,7} Of those sensors,

fluorescent chemosensors appear to be particularly attractive over the other methods due to their specificity, high sensitivity, high selectivity, and real-time monitoring with fast response times.⁷ However, Cu²⁺ presents an inherent problem for fluorescent sensing because of the likely quenching of the fluorescence by mechanisms inherent to paramagnetic species.⁸ Most of the classic and early-reported Cu²⁺ sensors generally show low sensitivity, and moreover, low selectivity.⁹ Additionally, most of the chemosensors are based on single emission intensity changes such as fluorescence quenching¹⁰ or enhancement,¹¹ which tend to be affected by a variety of factors such as instrument efficiency, probe molecule concentration, and micro-environment.¹²

To overcome these disadvantages, ratiometric fluorescent sensors have been well developed in recent years.¹³ Ratiometric fluorescent measurements observe changes in the ratio of the intensities of the emission at two wavelengths. Thus, ratiometric fluorescent sensors have important features that can be used to evaluate the analytical concentration and provide a built-in correction for environmental effects.¹² Among the various fluorophores, pyrene exhibits monomer–excimer dual emission wavelength fluorescence,¹⁴ and the

* Corresponding author. Fax: +81 952 28 8548; e-mail address: yamatot@cc.saga-u.ac.jp

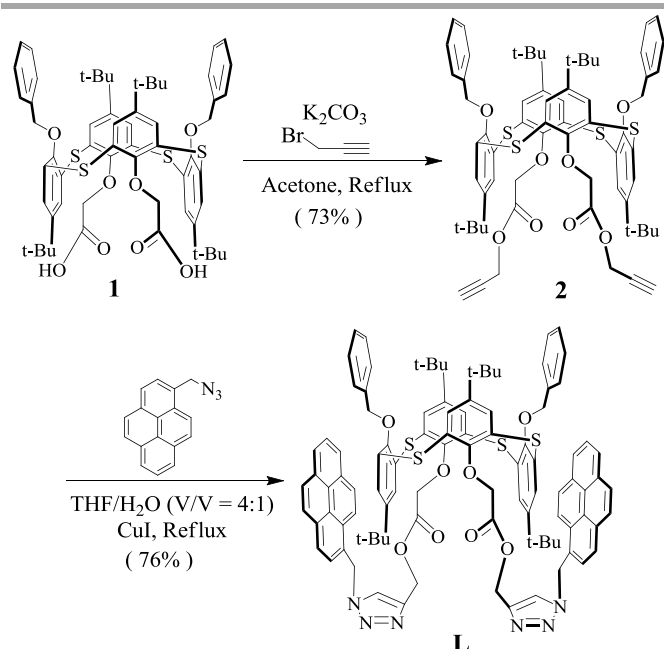
(T. Yamato).

fluorescence intensity ratio of the excimer to monomer emission (I_{Ex}/I_M) is sensitive to conformational changes of the pyrene-functionalized system.^{8a,15} Additionally, pyrene possesses photophysical properties that make it appropriate for such purposes due to its high fluorescence quantum yield, chemical stability, and long fluorescence lifetime.¹⁶ Consequently, pyrene has been employed as a fluorophore in this paper.

Based on our previous research,¹⁷ a good chemosensor not only contains an efficient fluorophore, but also needs to take into account the geometry of the coordination sites for a specific cation (or anion). In general, copper ion sensors use soft heteroatoms, such as nitrogen and sulfur, as electron donors to coordinate with the metal cation.¹⁸ Thiacalix[4]arenes are widely exploited as a molecular platform for many fluorescent chemosensors in the construction of selective binding sites given its structural rigidity, various conformations and given that it allows for the facile introduction of fluorophores.¹⁹ Recently, we have reported that a pyrenyl-linked triazole-modified thiacalix[4]arene chemosensor displayed high affinity for silver ion by changing the monomer and excimer emission of the pyrene moieties. However, other heavy metal ions, especially Cu^{2+} and Hg^{2+} can be also strongly quench both the monomer and excimer emission of pyrene.²⁰ We have also reported chemosensors with similar structures namely, pyrenyl-linked triazole-modified homooxacalix[3]arene. It was found that the chemosensor having acetate groups ($-CH_2COO^-$) linking the triazole groups to the homooxacalix[3]arene showed a higher selectivity than the other in which the triazole groups were linked directly to the lower rim oxygen atoms.²¹ Therefore, we hypothesized that by analogy, introducing similar acetate group-linkages between the triazolyl-pyrenyl groups and the thiacalix[4]arene should help to improve the selectivity. In the present work, therefore, the synthesis and properties of the fluorescent chemosensor **L**, derived from thiacalix[4]arene with pyrene as a subunit is reported.

2. Results and discussion

2.1. Synthesis

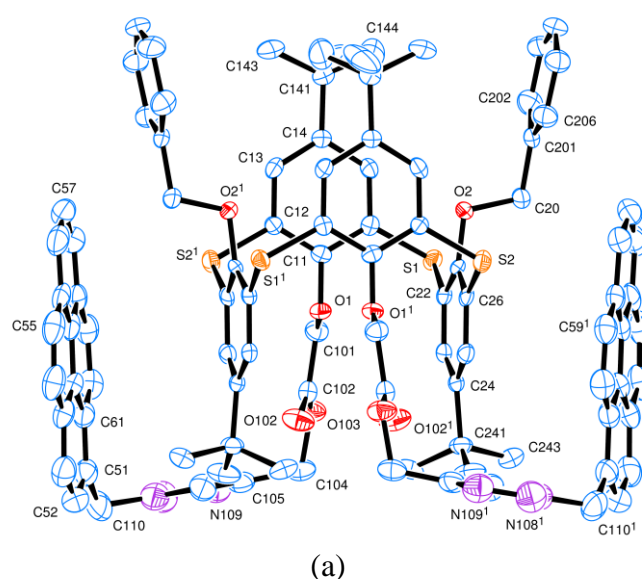


Scheme 1 The synthetic route of chemosensor **L**.

The synthesis of the parent compound **1** was carried out according to the published literature procedure.²² Recently, we described the synthesis of hexahomotrioxacalix[3]arene triacetic acid with propargyl alcohol, obtained by the Steglich esterification reaction with 1,3-dicyclohexylcarbodiimide (DCC) as a coupling reagent and 4-(*N,N*-dimethylamino)pyridine (DMAP) as a catalyst.²¹ However, in accordance with the above-mentioned method, we found that the reaction of the thiacalix[4]arene derivative **1**, even with a large excess of propargyl alcohol, only leads to the expected molecule **2** in a very low yield. Fortunately, an alternative, efficient route was found by using propargyl bromide (instead of propargyl alcohol) in the presence of K_2CO_3 as base, and we successfully obtained **2** in high yield (73%). Following this, the click reaction, *i.e.* Cu(I)-catalysed azide-alkyne cycloaddition, was used to synthesize the new chemosensor **L**. The synthetic route for this new chemosensor **L** is given in Scheme 1.

Compounds **2** and **L** were characterized by IR, 1H and ^{13}C NMR spectroscopy and by mass spectrometry. The 1H NMR spectrum of **2** exhibits two singlets for the *tert*-butyl protons at higher field, *viz* δ 0.84 and 1.26 ppm; two singlets for the aromatic protons at δ 7.15 ppm and 7.52 ppm, respectively, all of which is indicative of a C_2 -symmetric structure for the 1,3-*alternate* conformer. One terminal triple bond hydrogen signal is found at δ 2.47 ppm, which reveals that the propargyl group has been successfully introduced. In compound **L**, the proton signal of the propargyl hydrogens has disappeared, whilst a new singlet appearing at about δ 7.40 ppm is attributed to the protons of the newly formed triazole skeleton (for details, see the Supporting Information, Figures S1-S8).

X-ray quality pale yellow crystals of **L** were obtained by recrystallization from a MeOH/ $CHCl_3$ solution. ORTEP representations of the molecular structure of **L** are shown in Figure 1. It is clear that **L** adopts the 1,3-*alternate* conformation. There is a crystallographic twofold symmetry axis normal to the S_4 mean-plane, passing down the centre of the calixarene cage. Opposing phenyl rings, related by this symmetry, are essentially parallel with their normals only 0.14(9) and 1.16(12) $^\circ$ apart. These normals lie almost parallel to the S_4 plane, *i.e.* at angles of 89.93(7) and 89.42(6) $^\circ$ to the normal of that plane. There are turns in the long substituent chain on O(1) [and O(1')] so that the triazole ring lies nearly parallel to the S_4 mean-plane, and the pyrene group is folded back to form an outer sheath around the cage.



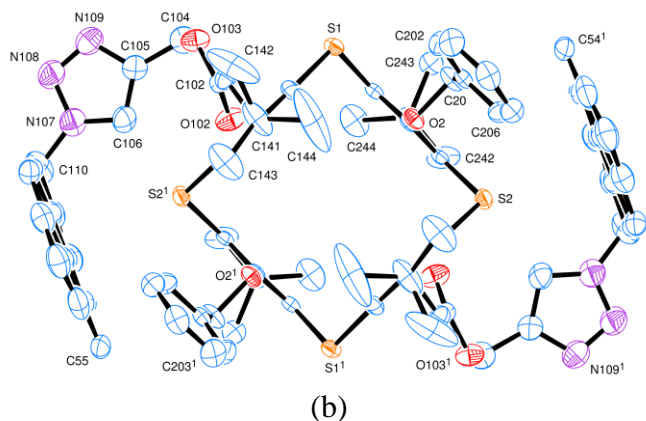


Figure 1. Single-crystal structure of **L**. (a) side view, (b) top view. Hydrogen atoms and the solvent water molecules have been omitted for clarity. Thermal ellipsoids are drawn at the 50% probability level.

2.2. Binding studies

The fluorescence spectra of **L** reveal a strong excimer emission at 484 nm and weaker monomer emissions at 379 and 397 nm (excitation wavelength 344 nm), with an intensity ratio of monomer to excimer emission (I_{M379}/I_{E484}) = 0.54. Among the various metal ions (Li^+ , Na^+ , K^+ , Cs^+ , Ag^+ , Zn^{2+} , Co^{2+} , Hg^{2+} , Pb^{2+} , Ni^{2+} , Cu^{2+} , Fe^{2+} and Fe^{3+} as their perchlorate salts.), chemosensor **L** displays highly selective ratiometric changes upon the addition of Cu^{2+} (Figure 2). As expected, the pyrene moiety serves successfully as a source of these ratiometric changes. The formation of an excimer band at 484 nm indicates a strong face-to-face π - π stacking between the two pyrene units. The relative intensity ratio of monomer to excimer emission (I_{M379}/I_{E484}) of the free sensor **L** is 0.54 and this was increased 228-fold to 123 upon the addition of 20 equiv. of Cu^{2+} (Figure 2b) and the formation of a **L**- Cu^{2+} complex. We postulate that the excimer quenching in sensor **L** is due to a conformational change that takes place during the binding of a Cu^{2+} ion between the nitrogen atoms of the triazole ring and the adjacent oxygen atoms. In this altered conformation, the coordination forces the pyrenyl groups to move away from one another thereby inhibiting the π - π stacking of the pyrene moieties which is necessary for the generation of the excimer emission.

In order to obtain more detailed complexation information for chemosensor **L** with the copper ion, fluorescence titration experiments were carried out. Interestingly, when we gradually increased the amounts of Cu^{2+} from 0 to 4 equiv., the fluorescence intensity of the excimer emission of **L** gradually decreased and was accompanied by an enhancement of the monomer emission in EtOH

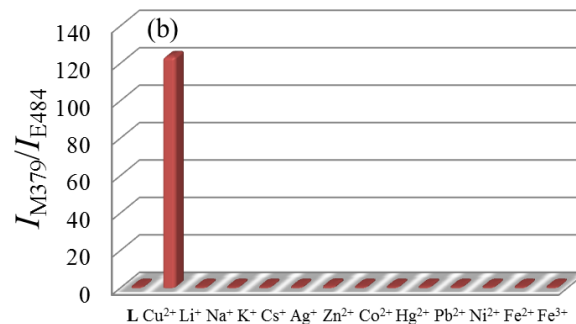
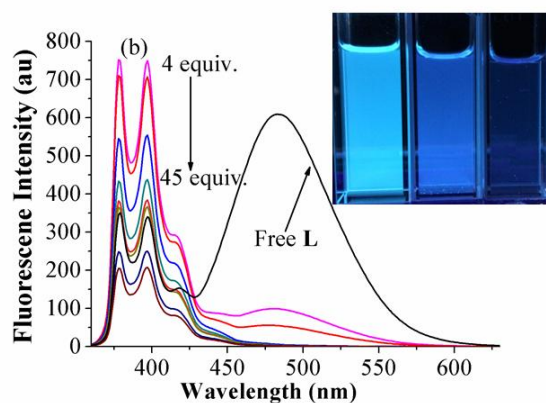
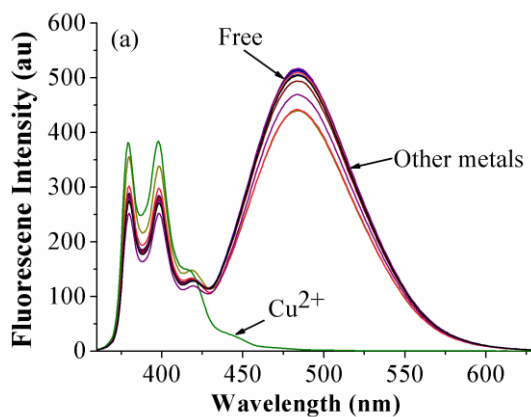
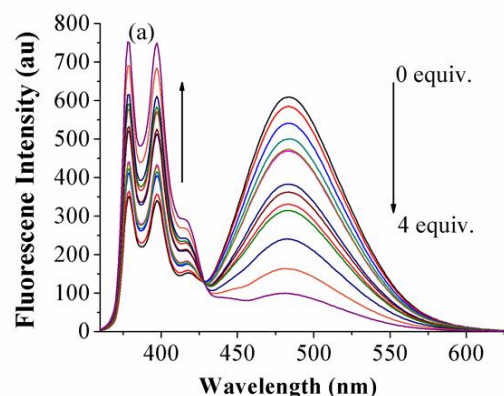


Figure 2. (a) Fluorescence spectra of the chemosensor **L** (1.5 μM) on addition of various metal ions (Li^+ , Na^+ , K^+ , Cs^+ , Ag^+ , Zn^{2+} , Co^{2+} , Hg^{2+} , Pb^{2+} , Ni^{2+} , Cu^{2+} , Fe^{2+} and Fe^{3+} , 30 μM) in EtOH solution at 298 K; (b) Ratiometric (I_{M379}/I_{E484}) selectivity of chemosensor **L** (1.5 μM) upon addition of various metal ions (30 μM) as their EtOH solutions. $\lambda_{\text{ex}} = 344$ nm.

solution (Figure 3a). However, when the concentration of Cu^{2+} was increased beyond 4 equiv. (5 equiv. to 45 equiv.), the fluorescence intensity of monomer emission exhibited a dramatic decrease (Figure 3b). These unique phenomena can also be visualized in the colour changes of the solution under UV light (Figure 3b inset) and is, to the best of our knowledge, is the first such case observed in thiocalixarene chemistry. A similar phenomenon was observed by Dabestani and coworkers in calix[4]arene.²³ They suggested that the gradual quenching of the emission from **L** observed at high concentrations of Cu^{2+} (Figure 3c) may be attributable to a medium effect caused by changes in the ionic strength of the solution. Additionally, the fluorescence of monomer emission quenching by the heavy atom (Cu^{2+}) in the chemosensor **L** generally can be attributed to a reverse PET (Photoinduced Electron Transfer)²⁴ from the pyrene unit to the nitrogen atoms of triazole ring or to a heavy atom effect.²⁵ In other words, the chemosensor **L** acts as an efficient ratiometric fluorescent chemosensor at low ion concentration or as a fluorescence quenching type chemosensor due to the PET and heavy atom effect at high ionic strength of the solution.



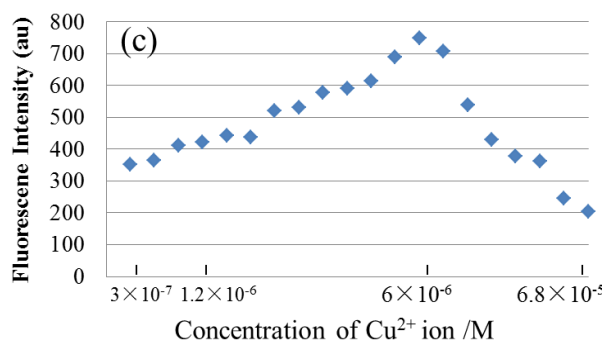


Figure 3. (a) Fluorescence intensity changes of **L** (1.5 μM) upon addition of increasing concentrations of Cu^{2+} in EtOH solution (0–4 equiv.); (b) (4–45 equiv.) at 298 K with an excitation at 344 nm; (c) Changes in the emission spectra (379 nm) of **L** (1.5 μM) in EtOH upon addition of Cu^{2+} ion (EtOH solution).

On the basis of the fluorescence titration experiments, the association constant (K_a)²⁶ for $\text{L}\cdot\text{Cu}^{2+}$ was determined to be $3.5 \times 10^5 \text{ M}^{-1}$ using a Benesi–Hildebrand plot (Figure S9, Supporting Information). The detection limit of the receptor was investigated, and a low detection limit of $1.44 \times 10^{-7} \text{ M}$ (Figure S10, Supporting Information) was observed. A Job plot²⁷ for the complexation revealed a 1:1 stoichiometry (Figure S11, Supporting Information). All of these results are clear evidence that chemosensor **L** possesses a high sensitivity and high selectivity for Cu^{2+} .

To investigate further the practical applicability of the chemosensor **L** as a Cu^{2+} ion selective fluorescent sensor, competitive experiments were carried out in the presence of Cu^{2+} ion (30 μM) mixed with Li^+ , Na^+ , K^+ , Cs^+ , Ag^+ , Zn^{2+} , Co^{2+} , Hg^{2+} , Pb^{2+} , Ni^{2+} , Fe^{2+} , Fe^{3+} at 30 μM . As shown in Figure S12, no obvious interference to the selective response of chemosensor **L** to Cu^{2+} in the presence of most of these metal ions. Accordingly, these observations suggested that chemosensor **L** can be used as a selective fluorescent sensor for the Cu^{2+} ion in the presence of most competitive metal ions.

Furthermore, in order to look further into the binding properties of chemosensor **L** with Cu^{2+} , ^1H NMR titration experiments were carried out in $\text{CDCl}_3 : \text{CD}_3\text{CN} = 10 : 1$ solution. The chemical shift changes for chemosensor **L** on complexation with Cu^{2+} are illustrated in Figure 4.

The peaks of H_a , H_b , H_c , H_d and H_e completely disappeared as

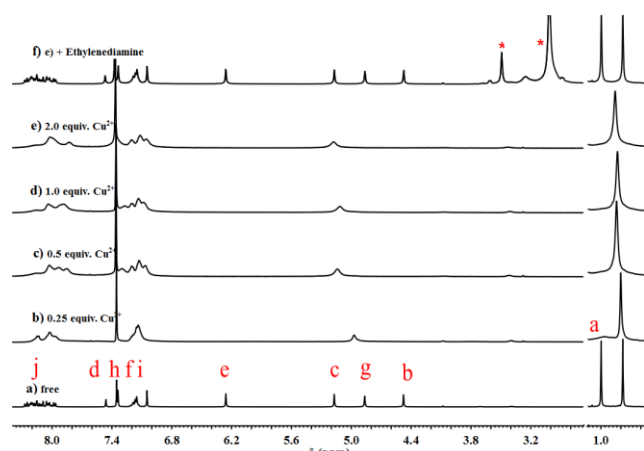


Figure 4. ^1H NMR spectral changes of Chemosensor **L** ($4 \times 10^{-3} \text{ M}$) on addition of $\text{Cu}(\text{ClO}_4)_2$ (400 MHz, $\text{CDCl}_3:\text{CD}_3\text{CN} = 10 : 1$). (a) Free **L**; (b) in the presence of 0.25 equiv. of $\text{Cu}(\text{ClO}_4)_2$; (c) in the presence of 0.5 equiv. of $\text{Cu}(\text{ClO}_4)_2$; (d) in the presence of 1.0 equiv. of $\text{Cu}(\text{ClO}_4)_2$; (e) in the presence of 2.0 equiv. of $\text{Cu}(\text{ClO}_4)_2$; (f) added 3 equiv. ethylenediamine to the solution of (e) * denoted the ethylenediamine peaks.

soon as 0.25 equiv. of Cu^{2+} were added, and the signals of the pyrene ring protons (H_j) and benzyl protons (H_f) were blurred; this was attributed to the paramagnetic effect of Cu^{2+} .⁸ The chemical shift of protons H_e ($-\text{OCH}_2\text{Benzyl}$) were shifted to downfield with $\Delta\delta = +0.31\text{ppm}$. This may be due to the protons H_e of free **L** is in the ring current shielding effect which is operating in the two thiacalixarene benzene rings (See the single-crystal structure of **L**, Figure 1a). However, when **L** complexed with Cu^{2+} , the conformation of **L** was changed which lead to the ring current shielding effect being decreased. This affected the protons H_g downfield shift close to the normal benzyl protons chemical shift (5.49ppm).²⁸ Peaks corresponding to the thiacalixarene benzene rings (H_h and H_i) underwent a slight chemical shift, which can be attributed to both the conformation changes and the paramagnetic effect of the Cu^{2+} (Figure 4). All of this evidence suggested that the 1,2,3-triazole and the adjacent oxygen were directly involved in coordinating with Cu^{2+} . There was no appreciable change in the signal positions on addition of 1.0 to 2.0 equiv. of Cu^{2+} to **L**, confirming a 1:1 binding stoichiometry for **L** and Cu^{2+} . Interestingly, it was observed that upon addition of ethylenediamine to a solution containing the $\text{L}\cdot\text{Cu}^{2+}$ complex, all of the disappeared peaks were immediately recovered (Figure 4f). This indicated that the complexation behaviour between **L** and Cu^{2+} ion was reversible.

IR spectroscopy was employed to give further evidence to support the possible complexation mode. The IR spectra of the complex ($\text{L}\cdot\text{Cu}^{2+}$) vs. the free host (**L**) are shown in Figure S13. In the spectrum of free **L**, there are two relatively strong absorptions (bands at 1770 and 1740 cm^{-1}) which are correspond to $-\text{COO}-$ group, which are dramatically changed to a weak absorption (band at 1743 cm^{-1}) after complexation with Cu^{2+} . A similar phenomenon also has been observed for the triazole group, bands at 1604 and 1588 cm^{-1} which disappear after complexation with Cu^{2+} . In other words, all of these evidences strongly indicate that Cu^{2+} is captured by these groups. The concept of Cu^{2+} complexation by the host chemosensor **L** is shown in Figure 5. Once the Cu^{2+} was captured by the nitrogen and oxygen atoms, the protons which are located in the adjacent area of the Cu^{2+} would be affected strongly by Cu^{2+} due to the inherent paramagnetism of Cu^{2+} , which led to the adjacent protons disappearing.

To better understand the binding properties of chemosensor **L** with Cu^{2+} , density functional theory (DFT) computational studies were carried out to determine the geometry-optimized energies of chemosensor **L** with Cu^{2+} ion. The starting structure was generated from the X-ray structure of **L**. The large distance between the nitrogen atoms of the triazole rings shown by the X-ray structure of the ligand **L** prevented effective binding, in the DFT-optimized structures between the Cu^{2+} and the two triazole units as evidenced by the ^1H NMR data (Fig. 4) was modified using

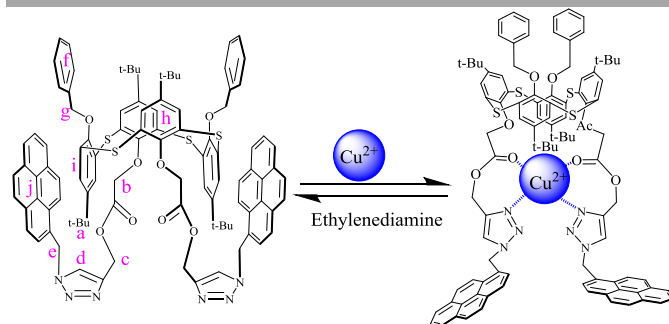


Figure 5. Plausible binding model of $\text{L}\cdot\text{Cu}^{2+}$ complex.

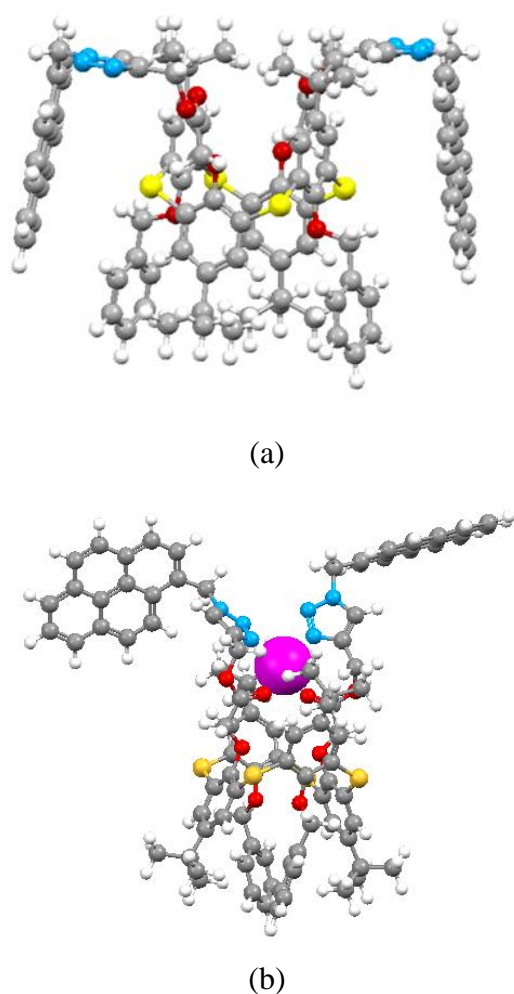


Figure 6. Geometry-optimized (ball-and-stick) structures of: a) **L** (from X-ray of **L**) and b) **L** \supset Cu^{2+} complex in gas phase. Colour code: Cu^{2+} = magenta, nitrogen = light blue, sulphur = yellow, hydrogen = white, carbon = dark grey and oxygen atom = red.

SpartanPro'10.^{29a} This was accomplished using the xyz coordinates obtained from the single-crystal structure of **L** for the complexation DFT study with Cu^{2+} ion. The generated structure of the ligand **L** was then imported into *Gaussian-09 rev D.01*^{29b} and the geometry optimizations using the B3LYP/6-31G(d) basis set were first conducted in the gas phase (Fig. 6) and then with chloroform-corrected geometry-optimization. Significant conformational changes were observed for the pyrene ring moieties of **L** after the complexation with Cu^{2+} , which induced the excimer quenching in chemosensor **L**. The conformation changes for **L** upon complexation with Cu^{2+} can be seen in Figure 6. Figure 6b shows the proposed structure of the **L** \supset Cu^{2+} complex. The optimized molecular geometry suggests that the Cu^{2+} binds in accord with the IR and ^1H NMR complex study. Cu^{2+} ion was located in the centre of fluorophore site, and the signal of the protons which surrounded Cu^{2+} ion will be strongly interfered due to the paramagnetic effect of the Cu^{2+} . The DFT B3LYP/6-31G(d) calculated apparent binding (or interaction) energies of modified **L** with Cu^{2+} were -1822 KJ/mol for the gas-phase and -971 kJ/mol in the CHCl_3 solvent system, respectively. The N-N distance between the triazole ring nitrogens decreases from 10.883 Å to 3.153 Å and 10.456 Å to 2.960 (Å) since the nitrogen atoms moved inwards after complexing **2** with Cu^{2+} in gas phase. The O-O distance the acetate group carbonyl oxygen's decreases from

10.595 Å to 2.724 Å after complexing **2** with Cu^{2+} in gas phase. (See the Supporting Information for details of the computational study, Table S1~S3 and Figure S14~15).

3. Conclusion

In summary, we have synthesized a new type of selective and sensitive fluorescent sensor having triazole rings as the binding sites on the lower rim of a thiacalix[4]arene scaffold in a 1,3-alternate conformation. The selective binding behaviour of chemosensor **L** has been evaluated by fluorescence spectra and ^1H NMR spectroscopic analysis. It was observed that chemosensor **L** acted as an efficient ratiometric fluorescent chemosensor at low ion concentration or as a fluorescence quenching type chemosensor due to the PET and heavy atom effect at high ionic solution strength. All the results suggested that chemosensor **L** is highly sensitive and selective for Cu^{2+} .

4. Experimental section

4.1 General

Unless otherwise stated, all reagents used were purchased from commercial sources and were used without further purification. Compound **1**¹⁹ was prepared following the reported procedures. All solvents used were dried and distilled by the usual procedures prior to use. All melting points (Yanagimoto MP-S1) are uncorrected. ^1H NMR and ^{13}C NMR spectra were recorded on a Nippon Denshi JEOL FT-300 NMR spectrometer and Varian-400MR-vnmrs400 with SiMe_4 as an internal reference: J-values are given in Hz. IR spectra were measured for samples as KBr pellets on a Nippon Denshi JIR-AQ20M spectrophotometer. Mass spectra were obtained with a Nippon Denshi JMS-HX110A Ultrahigh Performance mass spectrometer at 75 eV using a direct-inlet system. UV-vis spectra were recorded using a Shimadzu UV-3150UV-vis-NIR spectrophotometer. Fluorescence spectroscopic studies of compounds in solution were performed in a semimicro fluorescence cell (Hellma®, 104F-QS, 10 × 4 mm, 1400 μL) with a Varian Cary Eclipse spectrophotometer.

4.2. Materials

4.2.1. Synthesis of compound 2. A suspension of **1** (203 mg, 0.2 mmol) and K_2CO_3 (400 mg, 2.9 mmol) was heated at reflux for 1 h in dry acetone (20 mL), and a solution of propargyl bromide (345 mg, 2.9 mmol) in dry acetone (10 mL) was added. The reaction mixture was refluxed for 24 h. The solvents were evaporated and the residue partitioned between 10% HCl and CH_2Cl_2 . The organic layer was separated and dried (MgSO_4) and the solvents were evaporated. The residue was dried to afford the product **2** (180 mg, 72.7%) as a white solid. M.p.: 267–268 °C. IR ν_{max} (KBr)/ cm^{-1} : 3292, 3065, 3033, 2961, 2906, 2869, 2131, 1778, 1746, 1576 and 1498. ^1H NMR (400 MHz, CDCl_3) δ = 0.84 (18 H, s, *tBu*), 1.28 (18H, s, *tBu*), 2.47 (2H, s, *HCC*), 4.64 (4H, s, HCCCCH_2O), 4.76 (4H, s, OCH_2COO), 4.99 (4H, s, $\text{OCH}_2\text{Benzyl}$), 7.15 (4H, s, *ArH*), 7.19 (10H, s, *PhH*) and 7.52 (4H, s, *ArH*) ppm. ^{13}C NMR (100 MHz) δ 29.8, 30.2, 32.8, 33.2, 51.0, 65.7, 72.0, 74.1, 126.1, 126.5, 127.0, 127.2, 127.5, 129.8, 131.8, 136.9, 145.1, 145.3, 155.0, 157.2 and 166.1 ppm. HRMS (ESI-TOF): calcd for $\text{C}_{64}\text{H}_{68}\text{O}_8\text{S}_4$ [$\text{M} + \text{H}$]⁺ m/z = 1093.3875; found 1093.3961 [$\text{M} + \text{H}$]⁺.

4.2.2. Synthesis of receptor L. Copper iodide (20 mg) was added to a mixture of **2** (150 mg, 0.14 mmol) and 1-(azidomethyl)pyrene (108 mg, 0.42 mmol) in 25 mL THF/ H_2O (4:1)

and refluxed for 24 h. The resulting solution was cooled and diluted with water and extracted with CH_2Cl_2 . The organic layer was separated and dried (MgSO_4) and evaporated to give the solid crude product. The residue eluted from a column chromatography column of silica gel with CHCl_3 gave the desired product, **L** (170 mg, 76.1%) as colourless prisms. Mp: 231–232°C. IR ν_{max} (KBr)/ cm^{-1} : 3450, 3043, 2962, 2904, 2869, 1770, 1740, 1651, 1604, 1588 and 1497. ^1H NMR (400 MHz, CDCl_3) δ = 0.78 (18H, s, *tBu*), 1.00 (18H, s, *tBu*), 4.48 (4H, s, $-\text{OCH}_2\text{COO}-$), 4.87 (4H, s, $-\text{OCH}_2\text{Benzyl}$), 5.17 (4H, s, $-\text{TriazoleCH}_2\text{O}-$), 6.23 (4H, s, $-\text{CH}_2\text{Pyrene}$), 7.05 (4H, s, *ArH*), 7.16–7.18 (10H, m, *PhH*), 7.34(4H, s, *ArH*), 7.40 (2H, s, *Triazole-H*) and 7.94–8.24 (18H, m, *Pyrene-H*) ppm. ^{13}C NMR (100 MHz) δ 30.8, 30.9, 33.8, 34.0, 52.5, 57.8, 66.9, 73.1, 121.8, 123.6, 124.5, 125.0, 125.1, 125.9, 126.0, 126.4, 126.5, 127.1, 127.2, 127.4, 127.7, 127.9, 128.2, 128.4, 128.4, 129.2, 129.3, 130.5, 130.9, 131.2, 132.2, 133.0, 137.9, 142.9, 145.9, 146.0, 156.0, 158.1 and 167.7 ppm. HRMS (ESI-TOF): calcd for $[\text{M} + \text{H}]^+$ m/z = 1608.5815; found 1608.6492 $[\text{M} + \text{H}]^+$. Anal. Calcd for $\text{C}_{98}\text{H}_{90}\text{N}_6\text{O}_8\text{S}_4$: C, 73.20; H, 5.64; N, 5.23. Found: C, 71.95; H, 5.64; N, 4.96.

4.3. Crystal structure analysis of $L \cdot \text{H}_2\text{O}$

Crystal data: $\text{C}_{98}\text{H}_{90}\text{N}_6\text{O}_8\text{S}_4 \cdot \text{H}_2\text{O}$, $M = 1626.0$. Monoclinic, space group P2/n (equiv. to no. 13), $a = 17.4815(6)$, $b = 13.9971(5)$, $c = 18.1134(6)$ Å, $\beta = 109.991(3)^\circ$, $V = 4165.1(2)$ Å³. $Z = 2$, $D_c = 1.297$ g cm^{-3} , $F(000) = 1716$, $T = 140(1)$ K, $\mu(\text{Mo-K}\alpha) = 1.8$ cm^{-1} , $\lambda(\text{Mo-K}\alpha) = 0.71069$ Å.

Crystals are pale yellow, rectangular prisms. One, ca 0.43 x 0.14 x 0.10 mm, was mounted on a glass fibre and fixed in the cold nitrogen stream on an Oxford Diffraction Xcalibur-3/Sapphire3-CCD diffractometer, equipped with Mo-K α radiation and graphite monochromator. Intensity data were measured by thin-slice ω - and ϕ -scans. Total no. of reflections recorded, to $\theta_{\text{max}} = 22.5^\circ$, was 44921 of which 5417 were unique ($R_{\text{int}} = 0.086$); 3169 were 'observed' with $I > 2\sigma$.

Data were processed using the CrysAlisPro-CCD and -RED [19] programs. The structure was determined by the direct methods routines in the SHELXS program³⁰ and refined by full-matrix least-squares methods, on F^2 's, in SHELXL.³⁰ The non-hydrogen atoms were refined with anisotropic thermal parameters. Hydrogen atoms were included in idealised positions and their Uiso values were set to ride on the Ueq values of the parent carbon atoms. At the conclusion of the refinement, $wR_2 = 0.092$ and $R_1 = 0.086$ ³⁰ for all 5417 reflections weighted $w = [\sigma^2(F_o^2) + (0.0478P)^2]^{-1}$ with $P = (F_o^2 + 2F_c^2)/3$; for the 'observed' data only, $R_1 = 0.041$.

In the final difference map, the highest peak (ca 0.43 eÅ⁻³) was close to the water molecule, O(9).

Scattering factors for neutral atoms were taken from reference.³¹ Computer programs used in this analysis have been noted above, and were run through WinGX³² on a Dell Precision 370 PC at the University of East Anglia.

Crystallographic data for this structure have been deposited with the Cambridge Crystallographic Data Centre with code number CCDC 1063255. Copies of the data can be obtained, free of charge, on application to CCDC, 12 Union Road, Cambridge CB2 1EZ, UK [fax: 144-1223-336033 or e-mail: deposit@ccdc.cam.ac.uk].

Acknowledgments

This work was performed under the Cooperative Research Program of "Network Joint Research Center for Materials and Devices (Institute for Materials Chemistry and Engineering,

Kyushu University)". We would like to thank the OTEC at Saga University and the International Cooperation Projects of Guizhou Province (No. 20137005) for financial support. The EPSRC is thanked for a travel grant (to CR).

Supplementary data

Electronic Supplementary Information (ESI) available: Details of the ^1H , ^{13}C NMR, MS and IR spectra of compounds **2** and **L**; fluorescent and computational studies of **L** with Cu^{2+} . See DOI: 10.1039/b000000x/

References and notes

- (a) Que, E. L.; Domaille, D. W.; Chang, C. J. *Chem. Rev.*, 2008, **108**, 1517–1548; (b) Pontiki, E.; Hadjipavlou-Litina, D.; Chaviara, A. T.; Bolos, C. A. *Bioorg. Med. Chem. Lett.*, 2006, **16**, 2234–2237; (c) Gaggelli, E.; Kozlowski, H.; Valensin, D.; Valensin, G. *Chem. Rev.*, 2006, **106**, 1995–2044.
- Tapiero, H.; Townsend, D. M.; Tew, K. D. *Biomed. Pharmacother.*, 2003, **57**, 386–398.
- (a) Schaefer, M.; Gitlin, J. D. *Am. J. Physiol. Gastrointest. Liver Physiol.*, 1999, **276**, 311–314; (b) Huster, D. *Ann. N. Y. Acad. Sci.*, 2014, **1314**, 37–44.
- (a) Vonk, W. I.; Kakkar, V.; Bartuzi, P.; Jaarsma, D.; Berger, R.; Hofker, M. H.; Klomp, L. W.; Wijmenga, C.; Kampinga, H. H.; van de Sluis, B. *PLoS One*, 2014, **9**, e92408; (b) Xiao, G.; Fan, Q.; Wang, X.; Zhou, B. *Proc. Natl. Acad. Sci. U. S. A.*, 2013, **110**, 14995–15000; (c) Savelieff, M. G.; Lee, S.; Liu, Y.; Lim, M. H. *ACS Chem. Biol.*, 2013, **8**, 856–865; (d) McDonald, A. J.; Dibble, J. P.; Evans, E. G.; Millhauser, G. L. *J. Biol. Chem.*, 2014, **289**, 803–813.
- (a) Tak, W. T.; Yoon, S. C. *Korean J Nephrol.*, 2001, **20**, 863–871; (b) Cao, W.; Zheng, X. J.; Fang, D. C.; Jin, L. P. *Dalton Trans.*, 2015, **44**, 5191–5196.
- (a) Quan, L.; Sun, T. T.; Lin, W. H.; Guan, X. G.; Zheng, M.; Xie Z. G.; Jing, X. B. *J. Fluoresc.*, 2014, **24**, 841–846; (b) Chematea, S.; Sekar, N. *RSC Adv.*, 2015, **5**, 27282–27289; (c) Sutariya, P. G.; Pandya, A.; Lodha A.; Menon, S. K. *Analyst*, 2013, **138**, 2531–2535.
- (a) Jiang, P.; Guo, Z.; *Coord. Chem. Rev.*, 2004, **248**, 205–229; (b) Kim, J. S.; Quang, D. T. *Chem. Rev.*, 2007, **107**, 3780–3799; (c) Xu, Z.; Yoon, J.; Spring, D. R. *Chem. Soc. Rev.*, 2010, **39**, 1996–2006; (d) Kaur, P.; Singh, K. *RSC Adv.*, 2014, **4**, 11980–11999.
- (a) Silva, A. P. d.; Gunaratne, H. Q. N.; Gunnlaugsson, T.; Huxley, A. J. M.; McCoy, C. P.; Rademacher, J. T.; Rice, T. E. *Chem. Rev.*, 1997, **97**, 1515–1566; (b) Hu, Z.; Hu, J.; Cui, Y.; Wang, G.; Zhang, X.; Uvdal, K.; Gao, H. W. *J. Mater. Chem. B*, 2014, **2**, 4467–4472; (c) Cotruvo, J. A.; Aron, J. A. T.; Ramos-Torres, K. M.; Chang, C. J. *Chem. Soc. Rev.*, 2015, DOI: 10.1039/C4CS00346B.
- (a) Ni, X. L.; Zeng, X.; Redshaw, C.; Yamato, T. *Tetrahedron*, 2011, **67**, 3248–3253; (b) Patra, S.; Lo, R.; Chakraborty, A.; Gunupuru, R.; Maity, D.; Ganguly, B.; Paul, P. *Polyhedron*, 2013, **50**, 592–601; (c) Chavez-Crooker, P.; Garrido, N.; Ahearn, G. A. *J. Exp. Biol.*, 2001, **204**, 1433–1444.
- (a) Wang, J.; Long, L.; Xie, D.; Song, X. *Sensor. Actuat. B: Chem.*, 2013, **177**, 27–33; (b) Tang, B.; Yue, T.; Wu, J.; Dong, Y.; Ding, Y.; Wang, H. *Talanta*, 2004, **64**, 955–960.
- (a) Wu, S.; Zhang, K.; Wang, Y.; Mao, D.; Liu, X.; Yu, J.; Wang,

- L. *Tetrahedron Lett.*, 2014, **55**, 351–353; (b) Ma, L.; Cao, W.; Lin, J.; Zhang, M.; Yang, L. *Sensor Actuat. B: Chem.*, 2013, **181**, 782–786.
- 12 Wu, Y. S.; Li, C. Y.; Li, Y. F.; Tang, J. L.; Liu, D. *Sensor Actuat. B: Chem.*, 2014, **203**, 712–718.
- 13 (a) Thirupathi, P.; Lee, K. H. *Bioorg. Med. Chem. Lett.*, 2013, **23**, 6811–6815; (b) Das, S.; Sahana, A.; Banerjee, A.; Lohar, S.; Safin, D. A.; Babashkina, M. G.; Bolte, M.; Garcia, Y.; Hauli, I.; Mukhopadhyay, S. K.; Das, D. *Dalton Trans.*, 2013, **42**, 4757–4763; (c) Ingale, S. A.; Seela, F. *J. Org. Chem.*, 2012, **77**, 9352–9356.
- 14 Birks, J. B., *Rep. Prog. Phys.*, 1975, **38**, 903–974.
- 15 (a) Winnik, F. M. *Chem. Rev.*, 1993, **93**, 587–614; (b) Karuppanan, S.; Chambron, J. C. *Chem.–Asian J.*, 2011, **6**, 964–984.
- 16 (a) Winnik, F. M. *Chem. Rev.*, 1993, **93**, 587–614; (b) Yao, C.; Kraatz, H. B.; Steer, R. P. *Photochem. Photobiol. Sci.*, 2005, **4**, 191–199.
- 17 (a) Tomiyasu, H.; Zhao, J. L.; Ni, X. L.; Zeng, X.; Elsegood, M. R. J.; Jones, B.; Redshaw, C.; Teat, S. J.; Yamato, T. *RSC Adv.*, 2015, **5**, 14747–14755; (b) Jin, C. C.; Cong, H.; Ni, X. L.; Zeng, X.; Redshaw, C.; Yamato, T. *RSC Adv.*, 2014, **4**, 31469–31475; (c) Tomiyasu, H.; Jin, C. C.; Ni, X. L.; Zeng, X.; Redshaw, C.; Yamato, T. *Org. Biomol. Chem.*, 2014, **12**, 4917–4923; (d) Sun, Q.; Mu, L.; Zeng, X.; Zhao, J. L.; Yamato, T.; Zhang, J. X. *Sci. China Chem.*, 2015, **58**, 539–544.
- 18 (a) Jiang, Z.-T.; Deng, R.-R.; Tang, L. *Sensors Actuators B*, 2008, **135**, 128–132; (b) Weng, Y.-Q.; Yue, F.; Zhong, Y.-R.; Ye, B.-H. *Inorg. Chem.*, 2007, **46**, 7749–7755; (c) Cho, I. S.; Han, H.; Shim, J. H.; Lee, J. S.; Shin, J. H.; Cha, G. S.; Kim, B. H. *Tetrahedron Lett.*, 2010, **51**, 2835–2839; (d) Goswami, S.; Sen, D.; Das, N. K. *Org. Lett.*, 2010, **12**, 856–859.
- 19 (a) Morohashi, N.; Narumi, F.; Iki, N.; Hattori, T.; Miyano, S. *Chem. Rev.*, 2006, **106**, 5291–5316; (b) Kumar, R.; Lee, Y. O.; Bhalla, V.; Kumar, M.; Kim, J. S. *Chem. Soc. Rev.*, 2014, **43**, 4824–4870; (c) Song, M.; Sun, Z.; Han, C.; Tian, D.; Li, H.; Kim, J. S. *Chem.–Asian J.*, 2014, **9**, 2344–2357; (d) Zhao, J. L.; Tomiyasu, H.; Ni, X. L.; Zeng, X.; Elsegood, M. R. J.; Redshaw, C.; Rahman, S.; Georghiou, P. E.; Teat, S. J.; Yamato, T. *Org. Biomol. Chem.*, 2015, **13**, 3476–3483; (e) Zhao, J. L.; Tomiyasu, H.; Ni, X. L.; Zeng, X.; Elsegood, M. R. J.; Redshaw, C.; Rahman, S.; Georghiou, P. E.; Yamato, T. *New J. Chem.*, 2014, **38**, 6041–6049.
- 20 (a) Ni, X.-L.; Zeng, X.; Redshaw, C.; Yamato, T. *Tetrahedron*, 2011, **67**, 3248–3253; (b) Ni, X.-L.; Zeng, X.; Hughes, D. L.; Redshaw, C.; Yamato, T. *Supramolecular Chemistry*, 2011, **23**, 689–695.
- 21 (a) Ni, X. L.; Zeng, X.; Redshaw, C.; Yamato, T. *J. Org. Chem.*, 2011, **76**, 5696–5702; (b) Ni, X. L.; Wang, S.; Zeng, X.; Tao, Z.; Yamato, T. *Org. Lett.*, 2011, **13**, 552–555.
- 22 Perez-Casas, C.; Rahman, S.; Begum, N.; Zeng, X.; Yamato, T. *J. Inclusion Phenom. Macrocyclic Chem.*, 2008, **60**, 173–185.
- 23 (a) Ji, H. F.; Brown, G. M.; Dabestani, R. *Chem. Commun.*, 1999, 609–610; (b) Ji, H. F.; Dabestani, R.; Brown, G. M.; Hettich, R. L. *J. Chem. Soc., Perkin Trans. 2*, 2001, 585–591.
- 24 (a) Chang, K. C.; Su, I. H.; Senthilvelan, A.; Chung, W. S. *Org. Lett.*, 2007, **9**, 3363–3366; (b) Ojida, A.; Mito-oka, Y.; Inoue, M. A.; Hamachi, I. *J. Am. Chem. Soc.*, 2002, **124**, 6256–6258; (c) Choi, M.; Kim, M.; Lee, K. D.; Han, K. N.; Yoon, I. A.; Chung, H. J.; Yoon, J. *Org. Lett.*, 2001, **3**, 3455–3457.
- 25 Chae, M. Y.; Cherian, X. M.; Czarnik, A. W. *J. Org. Chem.*, 1993, **58**, 5797–5801.
- 26 (a) Benesi, H. A.; Hildebrand, J. H. *J. Am. Chem. Soc.*, 1949, **71**, 2703–2707; (b) Stern, O.; Volmer, M. *Phys. Z.*, 1919, **20**, 183–188.
- 27 Job, P. *Ann. Chim.*, 1928, **9**, 113–203.
- 28 Yamato, T.; Casas, C. P.; Yamamoto, H.; Elsegood, M. R. J.; Dale, S. H.; Redshaw, C. *J. Inclusion Phenom. Macrocyclic Chem.*, 2005, **54**, 261–269.
- 29 (a) Initial molecular modeling calculations using MMFF94 were performed using the *PC Spartan'10* software from Wavefunction Inc., Irvine CA.M.; (b) Frisch, M. J.; Trucks, G. W.; Schlegel, H. B.; Scuseria, G. E.; Robb, M. A.; Cheeseman, J. R.; Scalmani, G.; Barone, V.; Mennucci, B.; Petersson, G. A.; Nakatsuji, H.; Caricato, M.; Li, X.; Hratchian, H. P.; Izmaylov, A. F.; Bloino, J.; Zheng, G.; Sonnenberg, J. L.; Hada, M.; Ehara, M.; Toyota, K.; Fukuda, R.; Hasegawa, J.; Ishida, M.; Nakajima, T.; Honda, Y.; Kitao, O.; Nakai, H.; Vreven, T.; Montgomery, Jr. J. A.; Peralta, J. E.; Ogliaro, F.; Bearpark, M.; Heyd, J. J.; Brothers, E.; Kudin, K. N.; Staroverov, V. N.; Keith, T.; Kobayashi, R.; Normand, J.; Raghavachari, K.; Rendell, A.; Burant, J. C.; Iyengar, S. S.; Tomasi, J.; Cossi, M.; Rega, N.; Millam, J. M.; Klene, M.; Knox, J. E.; Cross, J. B.; Bakken, V.; Adamo, C.; Jaramillo, J.; Gomperts, R.; Stratmann, R. E.; Yazyev, O.; Austin, A. J.; Cammi, R.; Pomelli, C.; Ochterski, J. W.; Martin, R. L.; Morokuma, K.; Zakrzewski, V. G.; Voth, G. A.; Salvador, P.; Dannenberg, J. J.; Dapprich, S.; Daniels, A. D.; Farkas, O.; Foresman, J. B.; Ortiz, J. V.; Cioslowski, J.; Fox, D. J. *Gaussian 09, Revision D.01*; Gaussian, Inc., Wallingford CT, 2013.
- 30 Sheldrick, G. M. SHELX-97 – programs for crystal structure determination (SHELXS) and refinement (SHELXL), *Acta Crystallogr.*, 2008, **A64**, 112–122 and 2015, **C71**, 3–8
- 31 *International Tables for X-ray Crystallography*, ed. A. J. C. Wilson, Kluwer Academic Publishers, Dordrecht, 1992, vol. C, pp. 500, 219 and 193.
- 32 Farrugia, L. J. *J. Appl. Crystallogr.*, 2012, **45**, 849–854.

Synthesis, crystal structure and complexation behaviour study of an efficient Cu^{2+} ratiometric fluorescent chemosensor based on thiacalix[4]arene

Jiang-Lin Zhao^a, Hirotsugu Tomiyasu^a, Chong Wu^a, Hang Cong^{a,b}, Xi Zeng^b, Shofiu Rahman^c, Paris E. Georghiou^c, David L. Hughes^d, Carl Redshaw^e, Takehiko Yamato^{a,*}

Chemosensor **L** was capable of acting as an efficient ratiometric fluorescent chemosensor at low ion concentration or as a fluorescence quenching type chemosensor in high ionic strength solution.

